J Porous Mater (2008) 15:719–729
DOI 10.1007/s10934-007-9159-6

Mixed valences system in cobalt iron cyanide. Microporous structure stability

L. Reguera · E. Reguera · J. Balmaseda · J. Rodriguez-Hernandez · H. Yee-Madeira

Published online: 31 October 2007

Abstract Divalent transition metal hexacyanoferrates(III) have a microporous framework appropriate for separation and storage of small molecules. The nature of such porous framework is found in the existence of systematic vacancies of the building unit, the hexacyanoferrate octahedral block, $[Fe(CN)_6]$, in the material structure. The relatively low thermal stability appears to be the main limitation of these materials for such applications. In the as-synthesized material the available free volume is occupied by water which, can be removed by moderated heating but always involving decomposition of at least a small sample fraction. For cobalt a unique behavior has been observed. The heating of cobalt(2+) hexacyanoferrate(III) leads to an inner charge transfer to form the mixed valences Co(2+)Co(III) hexacyanoferrate(II,III) system. Since this inner oxidation–reduction reaction does not modify the coordination environments for the involved metals, the porous nature of the parent compound could be preserved and at the same time with a higher thermal stability related to the formation of the most stable ferrous species. The porous structure of the obtained material was evaluated from CO_2 adsorption, X-ray diffraction, thermogravimetric, and infrared and Mössbauer spectroscopic data. The heat-induced charge transfer is accompanied of a progressive fracture of the material crystallites and also of a decrease for the pore volume as detected by the CO_2 adsorption. For comparative purposes, a parallel study on a porous Prussian blue (ferric hexacyanoferrate(II)) species was carried out. The porous framework of this last material is also related to systematic vacancies of the hexacyanoferrate building block but without the mentioned heat-induced charge transfer effect. In this case the sample heating has no effect on the material porous properties.

Keywords Prussian blue analogue · Porous material · Porous framework · Mixed valences system · Adsorption

E. Reguera, H. Yee-Madeira—COFAA Fellows.

L. Reguera
Faculty of Chemistry, University of Havana, San Lázaro and L, 10400 Havana, Cuba

E. Reguera
Center for Applied Science and Advanced Technology of IPN, Mexico, DF, Mexico

E. Reguera (✉) · J. Rodriguez-Hernandez
Institute of Science and Technology of Materials, University of Havana, 10400 Havana, Cuba
e-mail: ereguera@yahoo.com

J. Balmaseda
Institute of Materials Research, National Autonomous University of Mexico, Mexico, DF, Mexico

H. Yee-Madeira
School of Physics and Mathematics of IPN, Col. Lindavista, Mexico, DF, Mexico

1 Introduction

The studied materials belong to a family of molecular structures known as Prussian blue (PB) analogues. Such structures result from the assembling of the octahedral anionic block, $[M^n(CN)_6]^{n-6}$, through a transition metal cation (T^{m+}) which forms relatively strong bonds at the N ends of the CN groups. The assembling process is usually carried out through soft chemical methods. The free space (porosity) of the obtained 3D network is related to the existence of systematic absence of the building block in the material structure or to the coordination adopted by the

outer metal (T) [1]. Porous PB analogues have values for the pore volume similar to those reported for some zeolites [2, 3] but with smaller access windows size. Such features have stimulated their evaluation for separation and storage of small molecules, among them, molecular hydrogen [4–6] and light hydrocarbons [1]. In addition, some hexacyanoferrates show interesting catalytic properties for production of biofuels and lubricants [7]. Compared with zeolites, cyanometallates have lower thermal stability and probably such feature has limited their extensive evaluation as porous materials. A deep understanding of the surface properties, pore accessibility, guest–host interactions and thermal stability of porous PB analogues could be useful to find applications for such open channel framework materials. Porous cyanometallates are also interesting as prototype of materials where the electronic structure of the host solid can be modified by adsorbed species, through guest–host interactions [8].

Within porous PB analogues, divalent transition metal hexacyanometallates(III), $T_3[M(CN)_6]_2$, have the largest values for the accessible free volume, related to 1/3 of the building block vacancies per formula unit. These materials crystallize with the cubic unit cell typical of PB [9] where the two metal centers (M, T) are found with octahedral coordination. In the as-synthesized material the free space due to the vacant sites is occupies by water molecules coordinated to the metal at the pore surface and also by weakly bonded waters stabilized within the pore through hydrogen bonding interactions with the coordinated ones. As average, the coordination sphere for the outer metal is formed by four N atoms plus two water molecules, $T(NC)_4(H_2O)_2$. Both coordinated and weakly bonded waters can be removed by moderate heating below 100 °C. These materials are free of large charge centers, alkaline ions for instance, to require high thermal energy to remove the crystal water. When all these water molecules are removed, a 3D network of cavities of about 8.5 Å (diameter) communicated by relatively smaller windows (the interstitial free spaces) of ca. 4.2 Å results [1, 10].

The thermal stability of $T_3[M(CN)_6]_2$ is closely related to the electronic structure for the inner metal (M). For M = Co, Rh, and Ir, where the metal t_{2g} orbitals are filled, the resulting material shows a relatively high thermal stability, above 250 °C [10]. A large availability of electrons at t_{2g} orbitals allows a pronounced π*-back donation from the inner metal (M) towards the CN groups and this enhances the M–CN bond increasing the building block stability. However, for M = Cr, Mn, and Fe, with three, four, and five electrons in t_{2g} orbitals, respectively, the thermal stability is lower. On heating these hexacyanometallates(III) are sensitive to structural and compositional changes. Hexacyanoferrates(III), for instance, decompose liberating CN^- groups which reduce the iron(III) atom to iron(II) giving hexacyanoferrates(II) and C_2N_2 [11]. In hexacyanoferrates(II) the iron atom has six electrons in t_{2g} orbitals and a relatively high thermal stability. The exception of such behavior for hexacyanoferrates(III) on heating is found for the cobalt(2+) complex salt [11, 12]. This compound shows a unique behavior on heating. In cobalt(2+) hexacyanoferrate(III), the reduction of the iron atom takes place through an inner charge transfer to form cobalt(III) hexacyanoferrate(II). This inner charge transfer is a progressive process and for a moderate heating a mixed valences system (MVS) of Co(2+)Co(III) hexacyanoferrates(II,III) is obtained, according to [12]:

$$Co_3[Fe(CN)_6]_2 \rightarrow (Co^{2+})_{3-x}(Co^{III})_x$$
$$[(Fe^{III})_{2-x}(Fe^{II})_x(CN)_{12}] \rightarrow (Co^{2+})(Co^{III})_2[Fe^{II}(CN)_6]_2$$

In such inner charge transfer the material porous framework must be preserved since the coordination environment for the involved metals does not change. For the resulting microporous compound a relatively higher thermal stability could be expected because a fraction of the iron atoms is found to be as low spin Fe(II). As far as we known, the properties of this mixed valences system as microporous material have not been evaluated, even when it could have attractive features. The aim of this contribution is the study of $(Co^{2+})_{3-x}(Co^{III})_x[(Fe^{III})_{2-x}(Fe^{II})_x(CN)_{12}]$ samples from CO_2 adsorption, X-ray diffraction (XRD), thermo-gravimetric (TG), and infrared (IR) and Mössbauer spectroscopic data in order to evaluate their properties as porous material, including the thermal stability. For comparative purposes, the results of a parallel study for a porous Prussian blue, $Fe_4[Fe(CN)_6]_3 \cdot xH_2O$, have been included and discussed. The porous network of this last compound is also related to systematic vacancies of the octahedral block, $[Fe(CN)_6]$, and with a relatively high thermal stability since the iron atoms are in their most stable electronic states for iron hexacyanoferrates. To the best of our knowledge, an analogue study for porous Prussian blue has not been reported before.

2 Experimental

Cobalt(2+) hexacyanoferrate(III) was obtained mixing aqueous solutions of cobalt(2+) nitrate and ferricyanic acid, this last one prepared in situ [13], in order to obtain a product free of accompanying alkaline ions. The obtained precipitate was filtered, washed several times with distilled water and then dried in air until it had constant weight. According to chemical analyses, the Co:Fe atomic ratio in the obtained solid is close to 3:2. Such atomic ratio corresponds to a compound with the following nominal formula unit, $Co_3[Fe(CN)_6]_2 \cdot xH_2O$, from now on labeled as Co_3Fe_2. The nature of the studied solid as

hexacyanoferrate(III) was corroborated from IR spectra. The PB sample used as reference compound was prepared using the same procedure but from solutions of potassium ferrocyanide and ferric chloride (in large excess). According to the Fe(3+):Fe(II) atomic ratio, estimated from Mössbauer spectroscopy [14], the formed solid corresponds to the insoluble modification of PB, $Fe_4[Fe(CN)_6]_3 \cdot xH_2O$; in the following IPB.

Two series of MVS samples were prepared. Series 1 (S1) corresponds to MVS species obtained heating Co_3Fe_2 for 2 h under a N_2 flow at 80, 100, 120, 140, and 160 °C, and then cooled within the used furnace. A heating rate of 5 °C/min. was used until to reach the temperature of heat-treatment. The average cooling rate remains below 2 °C/min. The used furnace takes at least 3 h in the cooling process until room temperature. Under these conditions $(Co^{2+})_{3-x}(Co^{III})_x[(Fe^{III})_{2-x}(Fe^{II})_x(CN)_{12}]$ is formed [12]. The samples of this series received a second heat treatment during the sample dehydration for the adsorption test, in dynamic vacuum (10^{-2} torr), and under the same heating conditions. The samples of S1 series will be identified as S1-80, S1-100, S1-120, S1-140, and S1-160. The results to be discussed for the structural characterization of this series correspond to the samples used in the adsorption experiments and then re-hydrated at room temperature for a weak in humid air. For the second series (series 2, S2), the mixed valences state system is formed during the sample (Co_3Fe_2) dehydration for the adsorption test. Before the structural characterization the samples of this second series (S2-80, S2-100, S2-120, S2-140, and S2-160) were also re-hydrated at room temperature in humid air for a week. The study of these two series (S1 and S2) allows us to shed light on the thermal stability of a previously formed MVS system and also on the effect of repeated heating cycles on the material properties. For the reference compound, IPB, where no heat-induced charge transfer is expected, the samples only received the dehydration heating previous to the adsorption experiment. This series is labeled as IPB-80, IPB-100, IPB-120, IPB-140, and IPB-160. S1, S2 and IPB series were characterized using the above mentioned techniques (XRD, IR, Mössbauer, and TG).

The IR spectra were recorded in Nujol mulls between KBr windows. On milling and pressing with KBr, hexacyanoferrates(III) reduce to hexacyanoferrates(II) [15]. Mössbauer spectra were run at room temperature in a constant acceleration spectrometer operated in the transmission mode with a $^{57}Co/Rh$ source. The obtained spectra were fitted using a least-squares minimization algorithm and pseudo-Lorentzian line shape in order to obtain the values for isomer shift (δ), quadrupole splitting (Δ), linewidth (Γ) and relative area (A). The values of δ are reported relative to sodium nitroprusside. The TG curves were recorded in the high-resolution mode using a TA Instrument (TG-2950 model) thermo-balance. XRD powder patterns were recorded in Bragg–Brentano geometry in a D8 Advance diffractometer (from Bruker) and monochromatic Cu Kα radiation in the (10–110)/2θ angular range, at a step of 0.025°/2θ with counting time of 20 s. The unit cell parameters were refined using the CellRef program [16] and the crystallite size was estimated from the peak width using the Scherrer equation [17].

The studied materials have relatively small pore windows size, about 4.5 Å. Related to this feature, in their N_2 adsorption isotherms at 77 K kinetic effects could be present, which have been reported for other PB analogues [1, 10]. From this fact the pore accessibility and stability of the material porous framework on heating were evaluated from CO_2 adsorption data collected at 0 °C. This probe molecule has a kinetic diameter of 3.45 Å (versus 3.85 Å for N_2) [18], which is smaller than the expected pore windows size. At 0 °C CO_2 molecule has a relatively high kinetic energy since this temperature is only 31 °C below its critical temperature [18]. This favors the CO_2 diffusion through small windows.

The CO_2 adsorption isotherms were collected using accelerated surface analysis and porosity equipment (ASAP 2010 model from Micromeritics). The adsorption data were evaluated combining the Dubinin–Astakhov (DA) and the Langmuir–Freundlich (LF) models [1, 10]. The limiting amount filling the micropores (n_p) is calculated from the LF solutions model and the obtained n_p value is then used as a non-variable parameter during the fitting of the experimental data according to the DA equation [19]:

$$n_{ad} = n_p \cdot \exp\{-[(RT/E_0) \cdot \ln(P_r^{-1})]^n\} \quad (1)$$

where n_{ad} is the amount adsorbed at a relative pressure P_r; n_p the limiting amount filling the micropores; E_0 the characteristic energy; n the heterogeneity parameter; R the universal gas constant; and T the temperature in Kelvin degree. The DA model has proved to be useful in the study of the adsorption in zeolites and carbons [20, 21] and also in porous cyanometallates [1, 2, 10, 22, 23]. The model was fitted to the experimental isotherms using a least-squares minimization routine. The pore volume estimation from CO_2 isotherms was carried out multiplying the respective n_p value by the molar volume in the liquid phase, 42.9 mL/mol for CO_2 [20].

The thermal effect on the porous framework was also evaluated comparing the variation in the adsorption potential (A) on the volumetric pore filling θ (n_{ad}/n_p) for different heating temperatures. The adsorption potential was estimated from the experimental data according to [19, 20, 24]:

$$A = -\Delta G = RT \cdot \ln(P_r^{-1}) \quad (2)$$

3 Results and discussion

3.1 On the crystal and electronic structure of the starting materials

The crystal structure and main properties of cobalt(2+) hexacyanoferrate(III) have already been reported [12]. Like other PB analogues, Co_3Fe_2 crystallizes with a cubic unit cell (Fm-3m). The calculated cell parameter results: a = 10.2666(2) Å. This value corresponds to the Co–N≡C–Fe–C≡N–Co chain length. This material is usually obtained with impurities of Co(III) and Co(2+) hexacyanoferrates(II). In addition to the intense ν(CN) absorption band at 2,160 cm^{-1}, due to –Co(2+)–N≡C–Fe(III)– chains in the nominal composition, the spectrum of the as-synthesized sample shows two weaker vibrations at 2,120 and 2,082 cm^{-1} (Fig. 1a, Table 1), which were ascribed to ferrous species. These two vibrations correspond to Co(III)–N≡C–Fe(II) and Co(2+)–N≡C–Fe(II) chains, respectively. The relatively high frequency for the Co(III) species indicates that the cobalt atom is found in low spin electronic configuration. These small ferrous fractions are formed during the synthesis process. As already mentioned, the hexacyanoferrate(III) anion has a natural trend to the reduction to give hexacyanoferrate(II) and in the presence of Co(2+) the reduction process takes place at expense of the cobalt atom oxidation to form Co(3+) with only one electron in e_g orbitals. In order to favor a stronger ligand–metal interaction, and a higher stability for the complex, that unpaired electron is transferred to the available t_{2g} hole giving a low spin configuration for the cobalt(3+) atom,

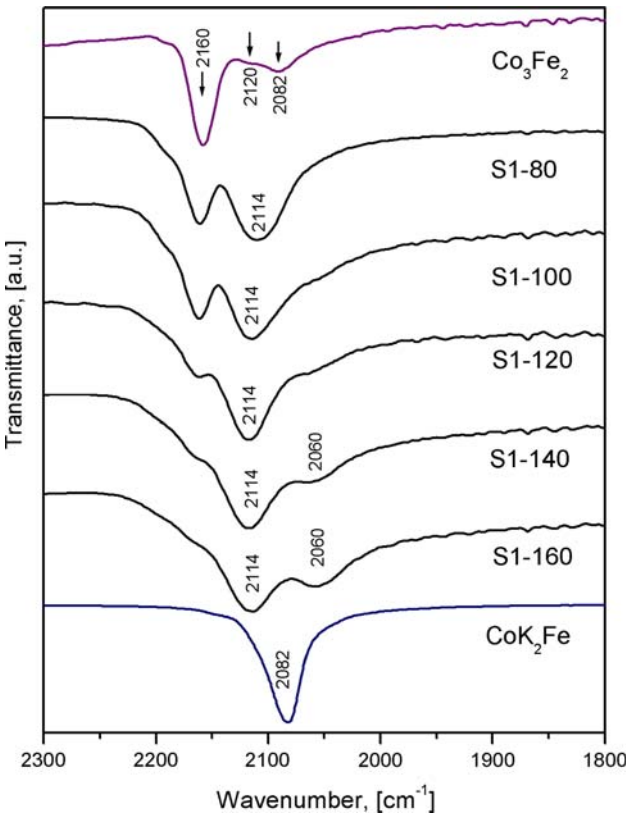

Fig. 1 IR spectra (ν(CN) vibration region) for series 1 samples. CoK_2Fe corresponds to a compound where only –Co(2+)–N≡C–Fe(II)–C≡N–Co(2+)– chains are found. The formation on heating of the $(Co^{2+})_{3-x}(Co^{III})_x[(Fe^{III})_{2-x}(Fe^{II})_x(CN)_{12}] \cdot xH_2O$ mixed valences system is detected as broad absorption band at 2,114 cm^{-1}. The IR spectra obtained for series 2 samples show a similar behavior on the temperature heating but without the 2,060 cm^{-1} band

Table 1 Observed IR frequencies (cm^{-1}) for the studied samples

Sample	ν(CN)	δ(FeCN)	ν(FeC)	ν(OH)	δ(HOH)
Co_3Fe_2	2,160; 2,120; 2,082	544	432	3,407 (Br.)	1,609
S1-80	2,160; 2,114 (Br.)	591–544	460–430	3,408 (Br.)	1,608
S1-100	2,160; 2,114 (Br.)	591–544	460–430	3,410 (Br.)	1,607
S1-120	2,160; 2,114 (Br.); 2,060	591–544	460–430	3,401 (Br.)	1,600
S1-140	2,160; 2,114 (Br.); 2,060	600–540	460–440	3,411 (Br.)	1,601
S1-160	2,160; 2,114 (Br.); 2,060	600–540	460–440	3,403 (Br.)	1,604
S2-80	2,160; 2,115 (Br.)	591–544	460–434	3,407 (Br.)	1,607
S2-100	2,160; 2,115 (Br.)	591–544	460–434	3,408 (Br.)	1,606
S2-120	2,160; 2,115 (Br.)	591–544	460–434	3,398 (Br.)	1,602
S2-140	2,160; 2,115 (Br.)	591–544	453	3,411 (Br.)	1,605
S2-160	2,160; 2,115 (Br.)	591–544	450	3,408 (Br.)	1,604
IPB	2,082	580	445	3,411 (Br.)	1,608
IPB-80	2,082	580	445	3,407 (Br.)	1,607
IPB-100	2,082	580	445	3,409 (Br.)	1,605
IPB-120	2,082	580	445	3,408 (Br.)	1,607
IPB-140	2,082	580	445	3,413 (Br.)	1,604
IPB-160	2,082	580	445	3,405 (Br.)	1,606

Br., broad

Co(III). Since the material has a polymeric nature, these last two ferrous species, Co(III)–N≡C–Fe(II) and Co(2+)–N≡C–Fe(II), appear together [25]. The ferrous impurities are also detected in the Mössbauer spectrum as a small single line contribution, which originates the small asymmetry observed in the quadrupole splitting doublet typical of cobalt(2+) hexacyanoferrate(III) (Fig. 2a). From the relative area of sub-spectra the as-synthesized sample composition was estimated to be 96% of cobalt(2+) hexacyanoferrate(III) while the remaining 4% corresponds to Co(III) and Co(2+) hexacyanoferrates(II) (Table 2). Such minor ferrous species were not detected by XRD.

According to the TG curve (Fig. 3), Co_3Fe_2 becomes anhydrous from 80 °C and then preserves certain stability up to 250 °C. The weight loss until 100 °C corresponds to a hydration degree of 12 water molecules per formula unit, 6 of them are coordinated and the remaining ones (6) are hydrogen bonded to the coordinated ones. On heating no differentiation between the evolution of coordinated and non-coordinated waters was detected (Fig. 3). Once the crystal water has been removed, the TG curve shows a slight weight loss which persists until the sample decomposition as a whole. Such slight weight loss was attributed to decomposition of the sample fraction of smaller particle size, which shows the lower thermal stability. PB analogues are usually obtained as nanometric size materials where a sample fraction has colloidal nature. According to the estimated XRD peaks width, the studied cobalt(2+) ferricyanide sample has an average crystallite size of about 48 nm.

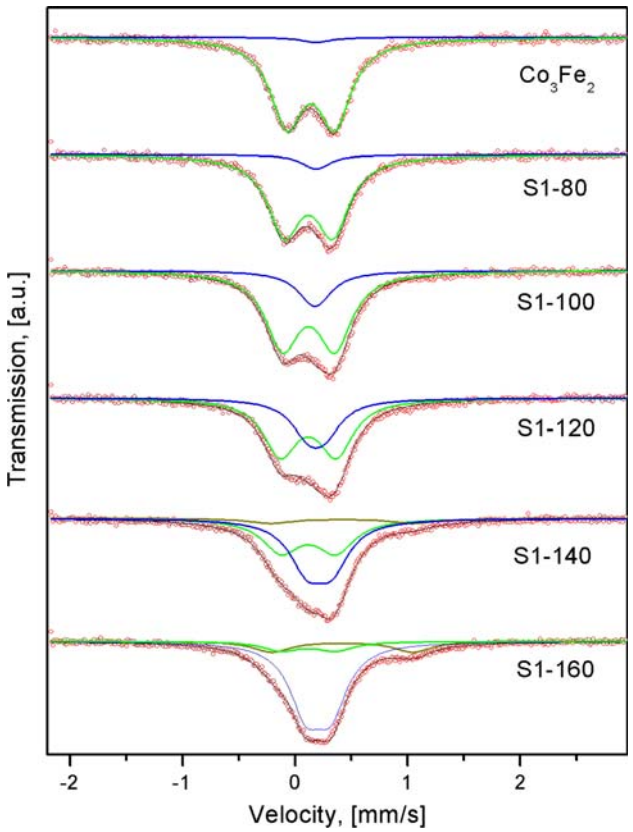

Fig. 2 Mössbauer spectra at room temperature for series 1 samples. The sample heating during the activation process leads to a progressive charge transfer to form $(Co^{2+})_{3-x}(Co^{III})_x[(Fe^{III})_{2-x}(Fe^{II})_x(CN)_{12}]$. An analog behavior was observed for series 2 samples but without the third doublet due to the partial sample decomposition on heating

Prussian blue corresponds to a generic name to designate ferric hexacyanoferrate(II), which exists in four slightly different modifications, with differences in composition and structure [14]. As already mentioned, the studied sample of PB corresponds to the IPB species, with an iron(3+) to iron(II) atomic ratio close to 4:3 (Table 2). The estimated Mössbauer parameters (Table 2) also correspond to a typical IPB [14]. The XRD powder pattern of this IPB sample was indexed as cubic (Fm-3m) with a cell edge size of: $a = 10.167(2)$ Å. The Fm-3m structural model in PB analogues supposes a random distribution of the vacant sites for the building block, $[M(CN)_6]$. In IPB such vacancies amount 25% of the available sites for the building block in the crystal structure. This leads to a mixed coordination sphere for the iron(3+) atom, with six coordinated waters per formula unit, $Fe(NC)_{4.5}(H_2O)_{1.5}$. The pore filling is completed with non-coordinated waters. The dehydration of IPB on heating has been reported [26]. On prolonged heating it becomes anhydrous from about 80 °C, without evidence of a definite difference between the evolution of coordinated and non-coordinated waters. According to the weight loss for the dehydration region, the studied sample of IPB was found to be with 14 water molecules per formula unit, which agrees with the reported crystal structure for this compound [27].

3.2 Structural changes in the studied materials on heating

XRD powder patterns of S1 and S2 series (not shown) correspond to the Fm-3m unit cell found for the parent Co_3Fe_2 compound. Figure 4a shows the evolution of the cell parameter on the temperature of heating for both S1 and S2 series. The charge transfer leads to formation of a solid solution of Co(2+) Co(III) hexacyanoferrate(III,II), where an increase in the amount of Co(III) and Fe(II) formed is detected as a progressive cell contraction (Table 3). Compared with Co(2+) and Fe(III), the effective crystal radii for Co(III) and Fe(II) are slightly smaller because their electronic configurations favor a stronger metal–ligand interaction. On the water removal certain cell contraction is expected [1, 8], however, on the sample re-hydration the inverse effect takes place [1, 10]. Since all

Table 2 Mössbauer parameters at room temperature for the studied materials

Sample	δ* (mm/s)	Δ (mm/s)	Γ (mm/s)	A (%)	Assignment
Co_3Fe_2	0.11	0.42	0.35	96	LS Fe(III)
	0.17	–	0.32	4	LS Fe(II)
S1-80	0.11	0.41	0.37	88	LS Fe(III)
	0.15	–	0.32	12	LS Fe(II)
S1-100	0.11	0.41	0.38	77	LS Fe(III)
	0.15	–	0.32	23	LS Fe(II)
S1-120	0.11	0.41	0.36	53	LS Fe(III)
	0.15	–	0.35	47	LS Fe(II)
S1-140	0.11	0.41	0.36	41	LS Fe(III)
	0.15	–	0.40	51	LS Fe(II)
	0.61	0.83	0.55	8	HS Fe(3+)
S1-160	0.11	0.41	0.36	11	LS Fe(III)
	0.15	–	0.43	73	LS Fe(II)
	0.62	0.82	0.55	16	HS Fe(3+)
S2-80	0.11	0.41	0.38	90	LS Fe(III)
	0.16	–	0.29	10	LS Fe(II)
S2-100	0.10	0.41	0.38	80	LS Fe(III)
	0.17	–	0.30	20	LS Fe(II)
S2-120	0.11	0.42	0.38	55	LS Fe(III)
	0.15	–	0.35	45	LS Fe(II)
S2-140	0.11	0.42	0.38	48	LS Fe(III)
	0.15	–	0.40	52	LS Fe(II)
S2-160	0.11	0.42	0.38	42	LS Fe(III)
	0.15	–	0.41	58	LS Fe(II)
IPB	0.12	–	0.30	43	LS Fe(II)
	0.64	0.51	0.43	57	HS Fe(3+)
IPB-80	0.12	–	0.32	44	LS Fe(II)
	0.64	0.50	0.42	56	HS Fe(3+)
IPB-100	0.12	–	0.34	42	LS Fe(II)
	0.64	0.51	0.43	58	HS Fe(3+)
IPB-120	0.12	–	0.30	44	LS Fe(II)
	0.64	0.52	0.44	56	HS Fe(3+)
IPB-140	0.12	–	0.29	43	LS Fe(II)
	0.64	0.53	0.43	57	HS Fe(3+)
IPB-160	0.12	–	0.30	42	LS Fe(II)
	0.64	0.52	0.45	58	HS Fe(3+)

* Isomer shift values are reported related to sodium nitroprussides. The fitting error in the values of δ, Δ and Γ remains below 0.01 mm/s. LS, low spin; HS, high spin

the XRD patterns were recorded on re-hydrated samples the observed cell contraction effect can only be attributed to the heat-induced charge transfer.

No significant difference between the cell contraction for both S1 and S2 series for heating temperatures up to 140 °C was observed. However, for the heating at 160 °C, the S1-160 sample shows the most pronounced cell contraction (Fig. 4a), suggesting the formation of a larger

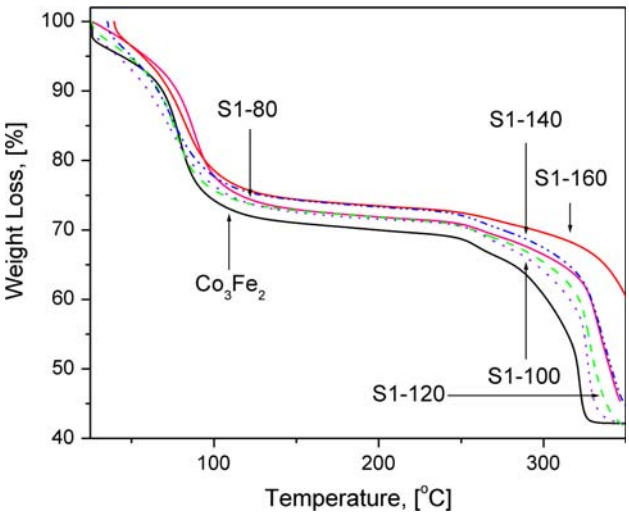

Fig. 3 Thermo-gravimetric curves for series 1 samples. The sample heating leads to a reduction in its water vapor adsorption capacity. For series 2 samples analogue TG curves were obtained

amount of Co(III) and Fe(II) species for both series. IR and Mössbauer spectra (discussed below) contribute to shed light on the nature of such behavior. The cell contraction on heating is accompanied by a parallel diffraction peaks broadening ascribed to a crystallite size reduction. Figure 4b shows the crystallite size variation with the temperature of heating. It seems that the heat-induced charge transfer to form the solid solution of Co(2+)Co(III) hexacyanoferrate(II,III) creates local strains that favor the fracture of the solid crystallites. Such local strains are probably related to the appearance on heating of Co(III)–N≡C–Fe(II)–C≡N–Co(III) chains of shorter length as compared with their analogues (Co(2+)–N≡C–Fe(III)–C≡N–Co(2+)) in the non-heated material. As larger is the amount of Co(III) and Fe(II) formed (smaller cell edge), more pronounced the crystallite size reduction results (Fig. 4b). For the IPB series, free of head induced charge transfer, no variation in the crystallite size on heating was observed (Fig. 4b).

The TG curves indicate that the dehydration temperature only has a slight dependence on the sample thermal history (Fig. 3). Such dependence could be attributed to several factors (a) appearance of Co(III) species at the pore surface, with an expected stronger interaction with the coordinated water molecules, (b) the observed cell contraction which reduces the available free space to accommodate water molecules, (c) decomposition of the sample fraction of smaller particle size. The observed shits towards high temperature for both the dehydration and decomposition temperatures can be attributed to the mentioned Co(III) appearance on the pore surface and formation of more stable chains (Co(III)–N≡C–Fe(II)–C≡N–Co(III)), respectively.

Table 3 Cell parameter and crystallite size variation on heating for the studied samples (S1, S2, and IPB series)

Sample	Cell edge (Å)	Crystallite size (A)	Sample	Cell edge (Å)	Crystallite size (A)	Sample	Cell edge (Å)	Crystallite size (A)
S1-27	10.289	475	S2-27	10.289	475	IPB-27	10.149	168
S1-80	10.273	276	S2-80	10.241	355	IPB-80	10.148	158
S1-100	10.195	222	S2-100	10.157	352	IPB-100	10.148	166
S1-120	10.135	200	S2-120	10.125	345	IPB-120	10.155	162
S1-140	10.001	174	S2-140	10.019	325	IPB-140	10.158	165
S1-160	9.907	150	S2-160	9.995	284	IPB-160	10.161	165

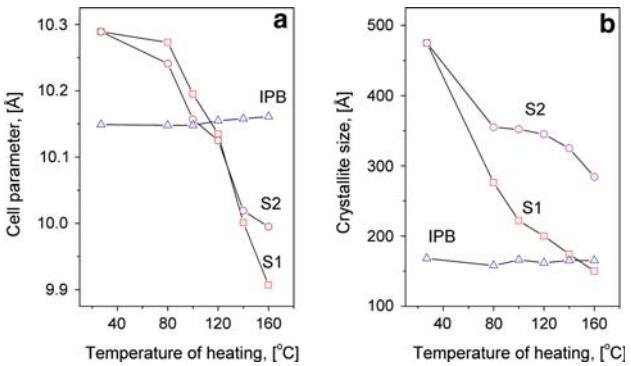

Fig. 4 Cell parameter (**a**) and crystallite size (**b**) change for the studied materials on heating. The charge transfer process to form $(Co^{2+})_{3-x}(Co^{III})_x[(Fe^{III})_{2-x}(Fe^{II})_x(CN)_{12}]$ leads to a cell contraction and to a reduction in the crystallite size, effects not observed for the reference compound (IPB)

The ν(CN) vibration of IR spectra from hexacyanometallates is an excellent sensor for the oxidation state and electronic configuration of both the inner and the outer metals in these compounds [11, 28–30]. From this fact, the IR spectra were used to sense the heat induced structural changes in the studied material. For the samples of S1 and S2 series the heat-treatment leads to an increase for the intensity of the ν(CN) bands at 2,120 and 2,082 cm^{-1}, which appear strongly overlapped to form a broad band around 2,114 cm^{-1} (Fig. 1). This broad band was attributed to formation of $(Co^{2+})_{3-x}(Co^{III})_x[(Fe^{III})_{2-x}(Fe^{II})_x(CN)_{12}]$. For S1-140 and S1-160 samples also a shoulder around 2,060 cm^{-1} is detected which was ascribed to a decomposition product with CN groups unlinked at the N end. An analogue low frequency ν(CN) vibration has been observed for other PB analogues due to their partial decomposition by heating [8].

Figure 2 shows the Mössbauer spectra for the samples of S1 series. In Table 2 the obtained parameters from the fitting of these spectra are collected. These spectra corroborate the results obtained from IR spectroscopy. The heat-induced inner oxidation–reduction reaction is observed as a decrease for the intensity of the quadrupole splitting doublet due to Co(2+) hexacyanoferrate(III) and appearance of a broad single line due to Co(III)–N≡C–Fe(II) and Co(2+)–N≡C–Fe(II) species formation. The difference of about 0.05 mm/s between the isomer shift values for the quadrupole doublet and that single line (Table 2) is conclusive regarding the electronic configuration of the involved iron atoms. To low spin Fe(III) corresponds a lower isomer shift value because in this case the iron atom has a smaller population of 3d electrons and a lower shielding effect for the s electron density at the iron nucleus. The progress of the charge transfer process on heating can be estimated from the obtained relative integral intensity (area of sub-spectrum) of these signals in the Mössbauer spectra [12]. For the samples heated at 140 and 160 °C an additional quadrupole splitting doublet of broad lines was observed. According to the isomer shift value found for this doublet, it corresponds to a high spin ferric species due to decomposition of a sample fraction. An analogue high spin Fe(3+) species has been found for other partially decomposed hexacyanoferrates(III) [31]. Such decomposition product probably has a low crystalline ordering because it is not detected by XRD. The beginning of the decomposition process was observed from the samples of 140 °C (S1-140). At this temperature the charge transfer process is even incomplete (Fig. 2, Table 2), however, the sample decomposition is already noted. A total charge transfer to form the expected end composition, $(Co^{2+})(Co^{III})_2[Fe^{II}(CN)_6]_2$, without evidence of thermal decomposition of the studied material, appears to be not possible.

According to IR, Mössbauer and XRD data, IPB appears to be stable within the temperature range considered (up to 160 °C). High spin iron(3+) at the N end and low spin Fe(II) at the C end of the CN bridge group are the most stable states for iron in cyanocomplexes. No variation in the IR spectra frequency values for the IPB series related to the heat-treatment was observed (Table 1), indicating that the electronic structure of IPB remains without changes on heating. The Fe(3+):Fe(II) atomic ratio, estimated from the Mössbauer spectra, was found to be close to 4:3 revealing that no oxidation–reduction reaction or partial sample decomposition have taken place during the sample heating. The calculated Mössbauer parameters, which sense the electronic configuration and coordination for the iron

atoms, show no variation on the IPB sample heating (Table 2). These IR and Mössbauer results are supported by XRD data. The XRD powder patterns for the heated IPB samples are similar to those obtained for the original compound, without significant variations for the cell edge and crystallite size (Fig. 4).

3.3 Carbon dioxide adsorption isotherms

The obtained CO_2 adsorption data (Fig. 5) are in correspondence with the microporous nature for the studied materials. The shape of these isotherms is similar to the ones reported for the families of divalent transition metals ferricyanides [1], cobalticyanides [10] and cubic nitroprussides [23], all these compounds with an analogue 3D network of interconnected pores. For S1 and S2 series the CO_2 amount that is adsorbed at a given P_r (relative pressure) value shows a marked dependence on the sample thermal history. However, independently of the sample thermal history, the CO_2 molecule participates of a relatively strong interaction with the material pore surface. Their slope at the low values of P_r appears particularly pronounced and at maximum P_r value that was reached (0.03), certain trend to the saturation is observed. The cavities (pores) of the studied materials are significantly larger than the kinetic diameter for the CO_2 molecule. Under these conditions the main contribution to the CO_2 molecule stabilization inside cavities probably comes from electrostatic interactions between the electric field gradient at the pore surface and the adsorbate quadrupole moment, with a minor contribution from Van der Waals type interactions.

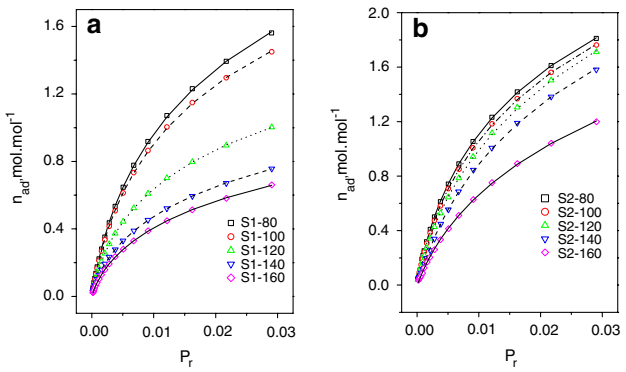

Fig. 5 Carbon dioxide adsorption isotherms for $(Co^{2+})_{3-x}(Co^{III})_x[(Fe_{III})_{2-x}(Fe^{II})_x(CN)_{12}]$ (series S1 and S2)

In Table 4 the results obtained from the fitting of these isotherms according to the combination of the LF–DA models are collected. The maximum values for the limiting amount filling the micropores (n_p) were found to be 3.9 CO_2 molecules per cavity for the S2-120 sample of the S2 series. It seems that at 120 °C, the sample reaches its optimal activation without a significant thermal decomposition. According to the molar volume for CO_2 (42.9 mL/mol), the adsorption of a CO_2 molecule requires 71 Å^3 and these 3.9 CO_2 represents an occupied volume of 277 Å^3. The cavities of the studied material has a diameter of about 8 Å for a cavity volume of 512 Å^3. This is equivalent to an occupation of about 50% of the cavity volume by CO_2 molecules. The CO_2 molecule has an ellipsoidal shape and within the cavity it must be oriented according to the local electric field gradient. Such orientation could be a limiting factor to attain a higher pore filling with CO_2 molecules. Analogues n_p values for CO_2 adsorption have been reported for other ferricyanides [1] and for cobalticyanides [10]. In addition to the orientation factor, the relatively high

Table 4 Results derived from the CO_2 adsorption isotherms fitting according to the DA model (n_p, the limiting amount adsorbed filling the micropores; E_0, characteristic energy; n, heterogeneity parameter; V_p, pore volume)

Sample	E_0 (kJ/mol)	n_p (mmol/g)	n_p (mol/mol)	n	V_p (cm^3/g)
S1-80	10.0 ± 0.1	4.9 ± 0.1	2.9 ± 0.1	2.20 ± 0.03	0.209 ± 0.004
S1-100	10.2 ± 0.1	4.4 ± 0.1	2.6 ± 0.1	2.24 ± 0.03	0.187 ± 0.003
S1-120	10.3 ± 0.1	3.0 ± 0.1	1.8 ± 0.1	2.18 ± 0.02	0.128 ± 0.001
S1-140	9.8 ± 0.1	2.4 ± 0.1	1.5 ± 0.1	2.02 ± 0.02	0.1047 ± 0.0009
S1-160	9.9 ± 0.1	2.2 ± 0.1	1.3 ± 0.1	2.04 ± 0.02	0.092 ± 0.001
S2-80	9.9 ± 0.1	5.7 ± 0.1	3.4 ± 0.1	2.20 ± 0.03	0.243 ± 0.004
S2-100	9.5 ± 0.1	6.0 ± 0.1	3.6 ± 0.1	2.07 ± 0.03	0.257 ± 0.004
S2-120	8.9 ± 0.1	6.4 ± 0.2	3.9 ± 0.1	1.97 ± 0.04	0.275 ± 0.009
S2-140	9.2 ± 0.2	5.6 ± 0.3	3.4 ± 0.2	2.08 ± 0.09	0.24 ± 0.01
S2-160	8.7 ± 0.2	4.7 ± 0.2	2.8 ± 0.1	2.00 ± 0.06	0.202 ± 0.009
IPB-80	10.7 ± 0.2	2.2 ± 0.1	1.9 ± 0.1	2.7 ± 0.1	0.093 ± 0.004
IPB-100	10.8 ± 0.1	2.5 ± 0.1	2.1 ± 0.1	2.76 ± 0.08	0.106 ± 0.003
IPB-120	10.4 ± 0.2	2.6 ± 0.1	2.2 ± 0.1	2.4 ± 0.1	0.111 ± 0.004
IPB-140	11.2 ± 0.1	2.4 ± 0.1	2.1 ± 0.1	2.72 ± 0.05	0.103 ± 0.002
IPB-160	10.9 ± 0.1	2.6 ± 0.1	2.2 ± 0.1	2.67 ± 0.04	0.110 ± 0.001

kinetic energy for the CO_2 at 0 °C could be contributing to that low values for the cavity volume occupation. From these facts, the estimated values for the pore volume, V_p (Table 4), can be used for comparative purposes within the studied series of compounds but not as an indicator for the material free space (pore volume).

For S2 series, the sample heating at the highest temperatures used, 140 and 160 °C, leads to a decrease for the n_p (or V_p) values, suggesting a reduction for the available or accessible pore volume or decomposition of a sample

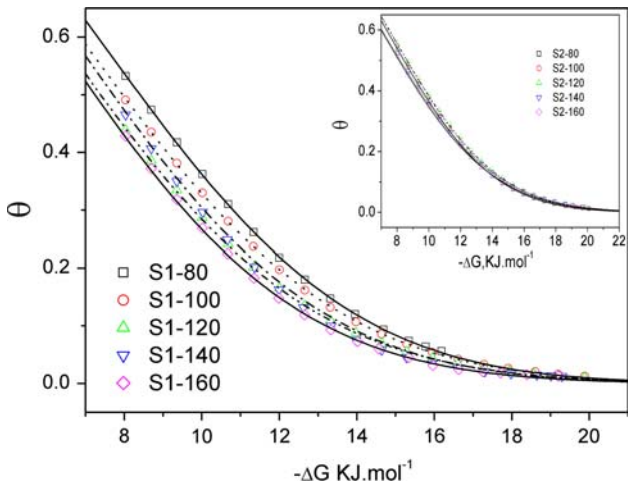

Fig. 6 Characteristic curves for carbon dioxide adsorption in series 1 (S1) and series 2 (S2, Inset) samples. For S2 series the adsorption potential results practically insensitive to the sample thermal history

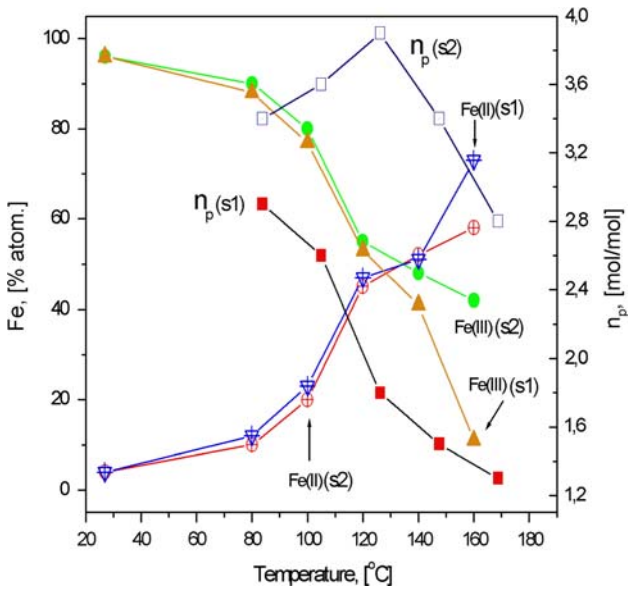

Fig. 7 Dependence of the relative population of Fe(II) and Fe(III) species as estimated from the fitted Mössbauer spectra, and of the maximum amount of adsorbed CO_2 molecules, on the heating temperature for S1 and S2 series. According to the observed dependences for S2 series the charge transfer process preserves the material porosity only within certain limits

fraction (Fig. 7, Table 4). For S1 series this effect even more pronounced. Such large variation for the n_p value in this series cannot be attributed to the unit cell contraction due to the heat-induced charge transfer. It can only be explained as due to formation of a material of non-porous nature or formation of porous structure of limited accessibility for the CO_2 molecule. Such hypothesis is supported by the remaining parameters calculated from the adsorption data. The obtained values for the heterogeneity parameter, n, in the DA model remain above 2 (Table 4), suggesting certain homogeneity for the adsorption potential that the CO_2 molecule is sensing. The value of this parameter is practically independent of the sample thermal history, suggesting that the CO_2 molecule is being adsorbed in pores of similar nature for all the studied samples, probably the sample fraction that has not been transformed plus a fraction of the formed solid solution. To this evidence also contributes the calculated values for the characteristic energy, E_0 (Table 4). In the DA model the E_0 parameter can be taken as a sensor for the strength of the guest–host interaction. Within a given series (S1 or S2) no significant variation for the E_0 was observed, and even, the values of this parameter are very similar for both series. The calculated characteristic curves for the CO_2 adsorption in these two series of mixed valence compounds (Fig. 6) provide conclusive evidence on the nature of the observed effect on heating. The shape of these curves is practically independently on the sample thermal history (Fig. 6). The adsorption potential (A) is similar for all the studied samples. Such behavior for the characteristic curves can be taken as evidence of a poor contribution of the formed mixed valence compound to the CO_2 adsorption in the studied material, at least above 120 °C of heating temperature.

Figure 7 shows the variation of low spin Fe(II) and Fe(III) species, in atomic percent, as estimated from the corresponding Mössbauer, and the obtained n_p values in mol/mol, as function of the temperature of heating. For S2 series the amount of CO_2 adsorbed increases up to the sample of 120 °C and then it decreases. However, up to 120 °C about 45% of the iron(III) has been reduced by the inner charge transfer. The mixed valence compound formed up to this temperature behaves as a porous material. However, the heating at a higher temperature leads to a reduction for the sample adsorption ability indicating that the formed mixed valences compound has a non-porous behavior or its pores become inaccessibility to the CO_2 molecule. For S1 series a drastic reduction for the CO_2 adsorption ability on heating was observed. The studied material is particularly sensitive to repeated cycles of heating, which favor the formation of a non-porous mixed valences compound. Such behavior cannot be attributed to the decomposition product since it only appears for a

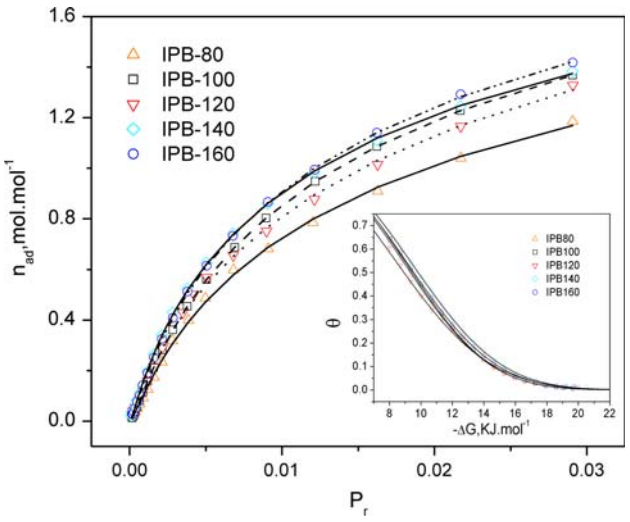

Fig. 8 Carbon dioxide adsorption isotherms and the corresponding characteristic curves (Inset) for insoluble Prussian blue activated in vacuum (10^{-2} torr) at different temperatures

heating temperature above of 120 °C (S1-140 and S-160 samples).

Figure 8 contains the collected CO_2 adsorption isotherms and the corresponding characteristic curves for the IPB series. These isotherms reveal a sample behavior on heating quite different to that discussed above for S1 and S2 series. For the IPB series an increase in the heating temperature leads to a larger CO_2 adsorption (n_p) size. Probably at 160 °C the IPB sample reaches the optimal activation, where all the crystal water has been removed. The free volume for IPB, related to $[Fe(CN)_6]$ vacancies, represents 75% of that expected for Co_3Fe_2. The obtained n_p value, in mol/mol (Table 4), for S2-120 and IPB-160 approximately parallels that expected ratio (3:4) for the accessible volume. The E_0 values for the IPB series are similar to those found for S1 and S2 series. This was ascribed to the nature of the porous framework in these two materials, which is related to vacancies of the hexacyanoferrate block. The higher value for the heterogeneity parameter (n) within the studied materials was obtained for the IPB series, probably due to the existence of a minor number of vacant sites per formula unit and a most tortuous diffusion path for the CO_2 molecule. No significant variation in the adsorption potential for the CO_2 molecule on the activation temperature for the IPB samples was noted (Fig. 8, Inset), an expected result since to the thermal treatment does not change the electronic and crystal structure of IPB.

4 Conclusions

The mixed valences system Co(III)Co(2+) hexacyanoferrate(III,II) formed during the heating of Co(2+) hexacyanoferrate(III) behaves as a porous material for temperatures of heating below 120 °C where only a partial charge transfer is induced. For a higher temperature of heating or repeated heating cycle, a non-porous mixed valences compound is obtained. The formation of a large fraction of hexacyanoferrate(II) not necessarily leads to an increase in the material thermal stability preserving the porous nature, as it was initially supposed. The heat-induced charge transfer is always accompanied of a shortening for the Co–N≡C–Fe–C≡N–Co chains detected as a cell contraction on the sample heating. Such chains length reduction generates local strains that induce the fracture of the involved crystallites. In this sense, the heat-induced charge transfer favors a reduction for the material crystalline ordering. According to the obtained data, above certain critical value for the charge transfer the porous framework collapses or the free space in the solid becomes inaccessible to the CO_2 molecule. For the porous Prussian blue studied such behavior was not observed. The XRD, IR, and Mössbauer data for the IPB series indicate that the crystal and electronic structures of this compound remain inalterable on heating, within the studied temperature range (up to 160 °C). In correspondence with such behavior the CO_2 adsorption data indicate that the porous framework of IPB is not affected by the sample heating, in contrast with above discussed results for cobalt(2+) hexacyanoferrate(III).

Acknowledgments L.R. acknowledges the support provided by the Latin American Network of Macro Universities students exchange program for his PhD studies. The partial financial support from CONACyT (Mexico) through the Project SEP-2004-C01-47070 is also acknowledged. The authors thank Dr. J.C. Llopiz who has facilitated the CO_2 adsorption data acquisition in ASAP 2010 equipment. The authors also thank E. Fregoso-Israel from IIM-UNAM (Mexico) by the TGA data recording.

References

1. J. Balmaseda, E. Reguera, J. Rodrgíuez-Hernández, L. Reguera, M. Autie, Microporous Mesoporous Mater. **96**, 222 (2006)
2. J. Balmaseda, E. Reguera, A. Gomez, B. Diaz, M. Autie, Microporous Mesoporous Mater. **54**, 285 (2002)
3. D.W. Breck, *Zeolite Molecular Sieves-Structure, Chemistry and Use* (John Wiley & Sons, 1974)
4. S.S. Kaye, J.R. Long, J. Am. Chem. Soc. **127**, 6506 (2005)
5. K.W. Chapman, P.D. Southon, C.L. Weeks, C.J. Kepert, Chem. Comm. 3322 (2005)
6. M.R. Hartman, V.K. Peterson, Y. Liu, S.S. Kaye, J.R. Long, Mater. Chem. **18**, 3221 (2006)
7. P.S. Sreeprasanth, R. Srivastava, D. Srinivas, P. Ratnasamy, Appl. Catal. A: Gen. **314**, 148 (2006)
8. R. Martínez-García, M. Knobel, E. Reguera, J. Phys.: Condens. Matter **18**, 11243 (2006)
9. A. Ludi, H.U. Gudel, Struct. Bond. **14**, 1 (1973)
10. J. Roque, E. Reguera, J. Balmaseda, J. Rodríguez-Hernández, L. Reguera, L.F del Castillo, Microporous Mesoporous Mater. **103**, 57 (2007)

11. R. Martínez-García, M. Knobel, E. Reguera, J. Phys. B **110**, 7296 (2006)
12. R. Martinez-Garcia, M. Knobel, G. Goya, M.C. Gimenez, F.M. Romero, E. Reguera, J. Phys. Chem. Solids **67**, 2289 (2006)
13. G. Brauer, *Handbook of Preparative Inorganic Chemistry*, 2nd ed., vol. 2 (Acad. Press, 1965), p. 1373
14. E. Reguera, J. Fernández-Bertrán, A. Dago, C. Diaz, **73**, 295 (1992)
15. J. Fernández, E. Reguera, Solid State Ionics **93**, 139 (1997)
16. J. Laugier, B. Bochu, 2006: CELREF V3 Cell parameters refinement program from powder diffraction diagram. http://www.inpg.fr/LMGP
17. A. Guinier, *X-ray Diffraction* (Dover Publications, 1994)
18. D.R. Lide (Ed.), *CRC Handbook of Chemistry and Physics*, 84th ed., (2003–2004)
19. M.M. Dubinin, in *Progress in Surface Science and Membrane Science*, ed. by D.A. Cadenheat (Academic Press, New York, 1975)
20. F. Stoeckli, Russ. Chem. Bull. Int. Ed. **50**, 2265 (2001)
21. M.H. Simonot-Grange, J. Chim. Phys. **84**, 1161 (1987)
22. P. Cartraud, A. Cointot, A. Renaud, J. Chem. Soc. Faraday Trans. 1 **77**, 1561 (1981)
23. J. Balmaseda, E. Reguera, A. Gomez, J. Roque, C. Vazquez, A. Autie, J. Phys. Chem. B **107**, 11360 (2003)
24. R. Roque-Malherbe, Microporous Mesoporous Mater. **41**, 227 (2000)
25. R. Martínez-García, M. Knobel, J. Balmaseda, H. Yee-Madeira, E. Reguera, J. Phys. Chem. Solids **68**, 290 (2007)
26. S.S. Kaye, J. R. Long, Catal. Today **120**, 311 (2007)
27. H.J. Buser, D. Schwerzenbach, W. Petter, A. Ludi, Inorg. Chem. **16**, 2704 (1977)
28. K. Nakamoto, *Infrared and Raman spectra of inorganic and coordination compounds* (John Wiley and Sons, New York, Toronto, Brisbane, Toronto, Singapore, 1992)
29. E. Reguera, J. Fernández, J. Duque, Polyhedron **13**, 479 (1994)
30. E. Reguera, J. Fernández, J. Balmaseda, Transit. Met. Chem. **24**, 648 (1999)
31. E. Reguera, J. Balmaseda, G. Quintana, J. Fernandez, Polyhedron **17**, 2353 (1998)